Electronic excitation of gas-phase furan molecules by electron impact

Romarly F. da Costa, Márcio H. F. Bettega, Marco A. P. Lima, Maria C. A. Lopes, Leigh R. Hargreaves, Gabriela Serna, and Murtadha A. Khakoo

Phys. Rev. A **85**, 062706 — Published 25 June 2012

DOI: 10.1103/PhysRevA.85.062706

Electronic excitation of gas-phase furan molecules by electron impact

Romarly F. da Costa

Centro de Ciências Naturais e Humanas,

*Universidade Federal do ABC, 09210-170, Santo André, SP, Brazil**

Márcio H. F. Bettega

Departamento de Física, Universidade Federal do Paraná,

Caixa Postal 19044, 81531-990, Curitiba, Paraná, Brazil

Marco A. P. Lima

Laboratório Nacional de Ciência e Tecnologia do Bioetanol (CTBE),

Centro Nacional de Pesquisa em Energia e Materiais (CNPEM),

Caixa Postal 6170, 13083-970, Campinas, SP, Brazil

Instituto de Física Gleb Wataghin, Universidade Estadual de Campinas,

Caixa Postal 6165, 13083-970, Campinas, SP, Brazil

Maria C. A. Lopes

Departamento de Física, ICE, Universidade Federal de Juiz de Fora,

36036-330, Juiz de Fora, MG, Brazil

Leigh R. Hargreaves, Gabriela Serna, and Murtadha A. Khakoo

Department of Physics, California State University Fullerton, Fullerton 92834, USA

(Dated: May 25, 2012)

Abstract

Experiments and *ab-initio* calculations of the differential and integral cross sections for the electronic excitation from the ground state $^1A_1$ to the $^3B_2$ and $^3A_1$ states of gas-phase furan molecules, by low-energy electron impact, were performed. Experimental differential cross sections were measured at incident electron energies between 5 to 15 eV and for scattering angles from 10° to 130°. The calculated cross sections were obtained using the Schwinger multichannel method implemented with pseudopotentials. The influence of channel-coupling and polarization effects is investigated through the comparison between three different models of scattering calculations, each one considering a distinct channel-coupling scheme. The comparison of experimental and calculated cross sections for electronically inelastic electron scattering by C_4H_4O molecules is found to be mostly reasonable. The existing discrepancies in this combined theoretical and experimental study help to illustrate difficulties in readily establishing reliable electronic excitation cross sections of polyatomic molecules by low-energy electrons.

PACS numbers: 34.80.Gs, 34.80.-i, 34.80.Bm

I INTRODUCTION

Electron-induced breakage of chemical bonds through dissociative electron attachment, a process mediated by the formation of temporary anionic states, has been recognized as a very efficient mechanism leading to the production of permanent lesions on DNA chains in the form of single- and double-strand breaks [1–5]. Much of the latest ongoing work on this subject has been devoted to the study of inelastic processes, more specifically, those involving electronic and/or vibrational excitations of the DNA basic constituents by impact of low-energy electrons [6–11]. In particular, the electronic excitation cross sections obtained in these studies revealed the presence of several core-excited resonances that appear at energies ranging typically from 5 eV to 10 eV. These findings are relevant because the formation of such short-lived negative ion states represents an alternative, and probably rather effective if compared to "one-particle" shape resonances, doorway for electron-induced damage to DNA. Thus, the determination of electronic excitation cross sections for biomolecules (such as the nitrogenous bases or the phosphate group) certainly represents a crucial step towards a deeper insight into the mechanisms of DNA damage by secondary electrons and establishes itself as a challenging task for experimentalists and theoreticians. On the experimental point of view, the difficulties for obtaining reliable cross sections are related to the resolution of the molecular spectra via energy loss assignments and widths of spectral features observed and also to the sensitivity of handling very low energy electrons in the electron spectrometer. From the theoretical perspective, there are also subtle aspects related to the description of such kind of processes, observed in applications involving relative small molecules with low-lying excited states, which should be considered so as to assess its influence on larger systems that also exhibit this specific characteristic.

Recent investigations concerning electron collisions with furan [12] and ethylene [13, 14] molecules demonstrated the importance of including polarization effects for an accurate description of the electronic excitation process. A particular feature that these two molecules have in common is the presence of a first excited triplet state lying at energies around 4 eV (see, for instance, Ref. [15]). As it is fairly known, taking the polarization of the target into account in the scattering calculations shows to be very important for description of the elastic process at the low energy range, especially with regard to the position of the resonances [16]. The results obtained in Refs. [12–14] indicated that the inclusion of these effects

also has strong influence on the electronic excitation process, leading to a significant change in the magnitude of the inelastic cross sections. In summary, these theoretical studies suggest that for molecular systems supporting resonances near to low-energy electronic thresholds, standard close-coupling calculations may produce incorrect results because of the lack of a proper treatment of the polarization effects which will give rise to misplaced resonances in the elastic coupled channel. For the $X^1A_g \rightarrow \tilde{a}^3B_{1u}$ transition in ethylene, the differential cross sections (DCSs) obtained at the two-channel close-coupling plus polarization level of approximation are in much better agreement with the experimental data compared to those obtained within scattering calculations where only channel-coupling effects were considered, as reported in [13, 14]. The two studies on electronic excitation of C_2H_4 by electron impact mentioned above have clarified the origin of the discrepancies between theoretical and experimental results observed for that system, which had remained without a satisfactory explanation for many years. In the case of furan, to our knowledge, there were no reported measurements or calculations with which to compare our electronically inelastic cross sections.

However it is worth noting that a careful review of the literature on the subject shows that, with the exception of electronic excitation, the number of studies related to electron collisions with furan is appreciable and has increased significantly in recent years. Early experimental works performed by van Veen [17] and by Flicker *et al.* [18, 19] are mainly concerned with the characterization of the electron-impact excitation spectra of furan, thiophene and pyrrole molecules by means of angle-differential energy loss spectroscopic measurements. Dissociative electron attachment to a series of five-membered heterocyclic compounds were investigated by Muftakhov and co-workers [20]. Using the mass spectroscopy technique these authors identified a number of structures which, for furan, appeared in the energy range from 3.5 eV to 10.7 eV and were assigned as core-excited Feshbach resonances having as parent states the first triplet excited state and a series of singlet excited states. Evidence of two negative ion resonances centered at around 1.8 eV and 3.1 eV, first reported by Modelli and Burrow [21], are in very good agreement with the assignments observed in elastic calculations carried out by Bettega and Lima [22], in a joint experimental-theoretical effort on elastic electron scattering conducted by Khakoo *et al.* [23] and, more recently, in the total cross section measurements performed by Szmytkowski *et al.* [24]. A broader structure having its maximum at about 8 eV was also reported in Refs. [22–24], but no attempts

to ascribe it to a more specific mechanism of electron capture was provided by these authors. Studies on resonant dissociative electron attachment to furan performed by Sulzer *et al.* [25] showed that during the resonant process several anionic fragments are formed. In particular, the results obtained in this work pointed out the existence of a core-excited shape resonance centered at 6 eV, which was also observed in the electron energy loss measurements done by Motte-Tollet *et al.* [26]. More recently, using the electron-impact optical excitation technique Dampc and Zubek [27] studied the production of excited fragments in furan. Dissociation and fragmentation processes considered in this work leads to formation of a number of electronically excited atomic as well as molecular fragments in the energy range between 15 eV to 95 eV. Finally, experimental differential cross sections for vibrational excitation structures in the electron energy loss spectra of furan in the range of 0 to 0.8 eV, were also determined at incident energy (E_0) values of 5.0, 6.0, 7.5, 9.0, 10.0 and 15.0 eV and angles in the range of 10° to 130° by Hargreaves *et al.* [28]. The measurements performed by these authors revealed the presence of a broad resonant feature at the E_0 value of about 7.5 eV for most of the vibrational energy loss features. This was consistent with the results obtained in Ref. [26].

Motivated by the growing interest in studies of electronic excitation of molecules by electron impact and also by the need for electron collision data for furan through which we could compare and relate our results, we decided to return to this matter and execute a series of measurements and *ab-initio* calculations for the electronic excitation of furan by low-energy electron impact. In this paper, we are focusing on the electron impact excitation of the $^1A_1 \rightarrow {}^3B_2$ and $^1A_1 \rightarrow {}^3A_1$ electronic transitions, and will also discuss the present theory as it appertains to an improvement compared to a previous model applied to elastic scattering. Here, *ab-initio* calculations were performed using the Schwinger multichannel method (SMC) [29] implemented with pseudopotentials (SMCPP) [30]. Elastic calculations were performed at the static-exchange and static-exchange plus polarization levels of approximation, whilst electronic inelastic calculations were carried out at different levels (up to nine) of channel-coupling, with and without the inclusion of polarization effects.

The organization of the paper is as follows. In the following two sections we describe the experimental setup with details of the furan excitation experiment. In the two sections following that theoretical aspects of the Schwinger multichannel (SMC) method are briefly reviewed and we present a summary of the computational details relative to the description

of furan target and to the scattering calculations. Thereafter, experimental and theoretical results obtained in this work are presented and discussed while in the final section, we summarize our findings with some conclusions.

II.1 EXPERIMENTAL SETUP

The experimental apparatus has been described in previous articles, e.g. Khakoo *et al.* [31], and so only a brief description will be given here. The electron gun and the detector employed titanium double hemispherical energy selectors and cylindrical lenses (also titanium), equipped with molybdenum apertures, used to transport, focus and collimate electrons emitted from a thoriated tungsten cathode onto a gas jet of furan molecules. The spectrometer system was baked to about 130°C by magnetically free biaxial heaters (ARi Industries model BXX06B41-4K). The analyzer's detector was a discrete dynode electron multiplier (Equipe Thermodynamique et Plasmas model AF151) with a background rate less than 0.01 Hz and a uniform detection efficiency for electron count rates up to 1 MHz. The remnant magnetic field in the collision region was reduced to around 1 mG by using a double μ-metal shield as well as a coil that reduced the vertical component of the Earths magnetic field.

Typical electron currents at the collision region were around 30 nA at all energies reported in this study. The electron beam current varied by less than 5% over the course of several days, subject to minor periodic re-tuning of the spectrometer to maintain the long term stablity. The energy of the beam, i.e. E_0, was established by determining the cut-off in the energy loss spectrum at zero residual energy. Alternatively, the beam energy could be calibrated against the dip in the He elastic-scattering cross section due to the 2 ^{2}S He resonance at 19.366 eV [32]. Both methods gave good agreement with each other regarding the determination of E_0. Typically the contact potential, so determined, stayed between 800 to 900 meV, with an uncertainty of 40 meV, over the multi-week course of the experiments. The energy resolution of the electron beam was approximately 70 meV.

Energy-loss spectra of the elastic peak were collected at fixed E_0 values and θ by repetitive multichannel-scaling techniques. The angular resolution of the electron analyzer was 2°, full width at half maximum. The effusive target gas beam was formed by flowing gas through a thin aperture source 0.3 mm in diameter described previously [33]. This source

was covered with carbon soot, using a pure acetylene flame, to reduce secondary electrons and placed 6 mm below the axis of the electron beam, incorporated into a movable source arrangement [34]. The movable gas source method determines background scattering rates expediently and accurately. The vapor pressure behind the source for furan was about 0.3 to 0.4 Torr and the pressure in the experimental chamber $\sim 4 \times 10^{-6}$ Torr. The operation of the experiment was entirely automated, the data acquisition computer controlled the angular positioning of the spectrometer, monitored the target gas drive pressure, modulated the gas beam and acquired the energy loss spectra. The gas beam temperature, determined by the apparatus temperature in the collision region, was about 130°C; however, in most of the gas handling copper tubing, the temperature was 24°C. The higher temperature was in the last 4 cm of the gas handling system before the gas exited into the collision region. Furan vapor was obtained from stabilized liquid furan (> 99.0% purity) which was degassed using multiple freeze-pump-thaw cycles.

II.2 EXPERIMENTAL DETAILS

Electron energy loss spectra (EELS) were taken at E_0 values of 5, 6, 7.5, 10 and 15 eV and for θ ranging from 10° to 130°. The spectrometer's transmission efficiency at different residual electron energies was determined by measuring EELS for nitrogen and then normalizing ratios of the inelastic to elastic peaks against those reported by Le Clair and Trajmar [35], who employed a time-of-flight energy analyzer which was essentially free of residual electron energy transmission effects. For this work, we used the data of Le Clair and Trajmar which covered all the valence bands below the $C^3\Pi_u$ state for E_0 values as low as 7.5 eV (their region I) as well as the $C^3\Pi_u$ bands (their region II) as a check. To determine the transmission efficiencies at $E_0 \leq 7.5$ eV, helium EELS were record at $E_0 = 34$ eV and $\theta = 90°$. The measured helium data was compared with the well-established inelastic differential cross-sections from convergent close coupling calculations by Fursa and Bray [36]. The transmission efficiencies were then determined using inelastic to inelastic ratios. For the helium ionization continuum the results of Schow *et al.* [37] were employed using the fact that the ionization continuum is flat at this particular E_0 and θ. An example of a furan EELS recorded in this work is shown in Figure 1, taken at an incident energy of 10 eV and scattering angle of 40°. The lowest lying $^3B_2$ and $^3A_1$ states are easily observed, as well as

several higher lying states, most of which are only partially resolved.

As can be seen from Figure 1, the $^3B_2$ and $^3A_1$ states are largely separated, but the $^3A_1$ state is fractionally overlapped with higher lying states. To unfold the spectrum, Gaussian peaks were fitted at the energy locations of the $^3B_2$ (3.97 eV) and $^3A_1$ (5.15 eV) states as reported by Guiliani *et al.* [38]. A third peak was also fitted at approximately 6.0 eV to represent the contribution of the $^1A_1$+$^1B_2$ higher energy loss state, in order to separate this contribution from the $^3A_1$ state. Higher lying states than the $^1A_1$+$^1B_2$ were not fitted for the present study. The fitting of the EEL spectrum was performed using an open-source data analysis and plotting software package (Qtiplot [39]). Once fitted the areas under the $^3B_2$ and $^3A_1$ peaks were compared with the area under the elastic peak (also fitted with a single Gaussian profile to remove any contribution from vibrationally inelastic scattering) and the measured elastic cross sections of Khakoo *et al.* [23], and corrected for spectrometer transmission using the method described above, to determine the final DCSs values.

III.1 THEORY

Although the SMC and SMCPP methods have been described in detail elsewhere [29, 30] we will present a summary of some details which are relevant for the discussion that follows. In the SMC method the resulting variational expression for the scattering amplitude in the body reference frame can be written as:

$$f(\vec{k}_i, \vec{k}_f) = -\frac{1}{2\pi} \sum_{m,n} \langle S_{\vec{k}_f} | V | \chi_m \rangle \left(d^{-1} \right)_{mn} \langle \chi_n | V | S_{\vec{k}_i} \rangle \ , \tag{1}$$

where the d_{mn} matrix elements are given by:

$$d_{mn} = \langle \chi_m | A^{(+)} | \chi_n \rangle \tag{2}$$

and the $A^{(+)}$ operator by:

$$\begin{aligned} A^{(+)} \ &= \ \frac{1}{2}(PV + VP) - VG_P^{(+)}V + \\ &+ \ \frac{\hat{H}}{N+1} - \frac{1}{2}\left(\hat{H}P + P\hat{H}\right) \ . \end{aligned} \tag{3}$$

In equations (1)-(3) the χ_m's, also known as configuration state functions (CSFs), are (N+1)-electron Slater determinants constructed from products of target states with one-particle wave functions:

$$\{|\chi_m\rangle\} = \{|\chi_{ij}\rangle\} = \mathcal{A}_{N+1}\left[|\Phi_i(1, ..., N)\rangle \otimes |\varphi_j(N+1)\rangle\right] \tag{4}$$

where $|\Phi_i\rangle$ are N-electron Slater determinants obtained by single excitations from the occupied (hole) orbitals to a set of unoccupied (particle) orbitals. As before, $|\varphi_j\rangle$ is represented by an one-electron wave function and $\mathcal{A}_{N+1}$ is the antisymmetrizing operator which accounts for the projectile electron's indistinguishability with the target electrons. From these products, only overall doublet states are retained if the target is a closed shell system, as discussed in Ref. [40]. $S_{\vec{k}_{i(f)}}$ is an eigenstate of the unperturbed Hamiltonian H_0, given by the product of a target state and a plane wave with momentum $\vec{k}_{i(f)}$; V is the interaction potential between the incident electron and the target; $\hat{H} \equiv E - H$ is the total energy of the collision minus the full Hamiltonian of the system, with $H = H_0 + V$; P is a projection operator onto the open-channel electronic space of the target:

$$P = \sum_{l \in \text{open}} |\Phi_l\rangle\langle\Phi_l| \tag{5}$$

and $G_P^{(+)}$ is the free-particle Green's function projected on the P-space. In our applications of the SMCPP method we have been using the norm-conserving pseudopotentials of Ref. [41] in order to represent the inner electrons close to the nuclei, as described in Ref. [30].

The analysis for numerical stability of the present calculations is performed through a check procedure originally developed to investigate the origin of unphysical resonances appearing in positron-N_2 calculations [42]. Adapted to the case of electron-molecule scattering [40] the analysis begins with the diagonalization of the matrix elements of the $\tilde{V}$ operator:

$$\tilde{V} \equiv \frac{1}{2}(PV + VP) + \frac{\bar{H}}{N+1} - \frac{1}{2}\left(\bar{H}P + P\bar{H}\right) \ , \tag{6}$$

where V, P have already been defined and $\bar{H} = \hat{H}$, calculated at a fixed energy. A next step consists in the identification and removal of the configurations weakly coupled by this average potential, that is, the eigenvectors associated to the eigenvalues near to zero of the equation $\tilde{V} \mid \tilde{\chi}_m\rangle = v_m \mid \tilde{\chi}_m\rangle$. The $\tilde{\chi}_m$'s are then used as a new (N+1)-electron basis functions.

III.2 COMPUTATIONAL DETAILS

Before starting the description of the technical aspects related to the computational procedures used to calculate the scattering amplitudes of interest for this study, we believe it is important to highlight some general aspects that contributed in defining the level of

approximation through which present calculations were performed. As it is fairly known, the theoretical modeling of electron collisions with molecules is a very complex task and, in order to get an appropriate description of this process we need to have a good balance between several aspects, such as: (i) a suitable choice of basis set functions to be used in the expansion of bound/excited target states and continuum scattering orbitals; (ii) an adequate treatment of polarization effects, which account for the distortion of the target's electronic cloud due to the presence of the incident electron and which are very important at low impact energies; and (iii) the inclusion of multichannel coupling effects describing the competition among all states that become energetically accessible to the target during the collision. Due to computational limitations, the use of approximations are necessary and specific choices related to each one of the aspects mentioned above (such as number of basis set functions, amount of polarization, number of coupled-channels, etc.) need to be made so as to maintain the compromise between a sufficiently complete description of the problem in question and the ability to carry out the computational calculations.

In the present work, three different models were used to study the electronic excitation of furan by electron impact. In all these models, the ground state was computed in the Hartree-Fock approximation. Bound state and scattering calculations were performed within the C_{2v} point group at the experimental equilibrium geometry [43] defined by the bond lengths R(O–C_3)=R(O–C_4)=1.362 Å, R(C_1–C_2)=1.434 Å, R(C_1–C_3)=R(C_2–C_4)=1.361 Å and R(C_1–H_1)=R(C_2–H_2)=R(C_3–H_3)=R(C_4–H_4)=1.076 Å; and by the angles θ(C_3–O–C_4)=106.6 degrees, θ(O–C_3–H_3)=θ(O–C_4–H_4)=115.9 degrees and θ(C_3–C_1–H_1)=θ(C_4–C_2–H_2)=127.9 degrees. Furan is a planar molecule in its electronic ground state and presents two fold axis of rotation that contains the oxygen atom and two vertical planes of symmetry (Figure 2) leading, as a result, to four irreducible representations labeled as A_1, A_2, B_1 and B_2 symmetries. The basis set employed within the Hartree-Fock approximation in our study was the same as the one used in the calculations presented in our previous joint experimental-theoretical work on elastic electron scattering from furan [23] and consists of square-integrable functions generated by a variational method [44]. For carbon atoms the basis set is composed by $5s5p2d$ uncontracted Cartesian Gaussian (CG) functions with exponents 12.49628, 2.470286, 0.614028, 0.184028, 0.039982, for the s–type functions; 5.228869, 1.592058, 0.568612, 0.210326, 0.072250, for the p–type functions and 0.603592, 0.156753 for the d–type functions. Oxygen atoms are described by a $5s5p2d$ set of

uncontracted CG functions with exponents 16.05878, 5.920242, 1.034907, 0.316843, 0.065203 for the s–type functions; 10.14127, 2.783023, 0.841010, 0.232940, 0.052211 for the p–type functions and 0.756793, 0.180759 for the d–type functions. For hydrogen atoms we used the $4s$ (contracted to $3s$) basis set of Dunning [45]. The dipole moment obtained with this basis set was 0.85 D which is in reasonable agreement with the experimental value of 0.66 D.

With regard to the description of multichannel coupling effects, in the three models considered here, the scattering calculations were performed at a nine-state close-coupling level of approximation and the states used in the composition of the space of coupled-channels, as well as its corresponding threshold energies, were obtained according to the minimal orbital basis for single configuration interactions (MOB-SCI) strategy [40]. The main purpose in using this strategy was to provide a good description of the first (few ones) excited states of the target in terms of the SCI technique while keeping the size of the associated pseudo-state space as minimum as possible. As discussed before, the idea behind the use of this procedure was based on the fact that an excited state constructed from an improved virtual orbital (IVO) [46], and calculated for a specific hole orbital, is equivalent to a complete single-excitation configuration interactions (SCI) calculation out of the same hole orbital that generates the IVO. In the case of furan, as will be explained below, it is not completly equivalent because in describing the excited states of interest to the present study it was necessary to use IVOs coming from two distinct occupied orbitals. In practice, the implementation of the MOB-SCI strategy used in the present study was undertaken as follows. By running a full SCI calculation we found that the description of the $^3B_2$ state was mainly due to contributions of hole-particle transitions of the type $b_1 \rightarrow a_2$ and $a_2 \rightarrow b_1$. Similarly, in describing the $^3A_1$ state we observed that contributions from hole-particle transitions of the type $b_1 \rightarrow b_1$ and $a_2 \rightarrow a_2$ were strongly coupled to each other. Now, aiming to investigate the influence of different multichannel coupling schemes on the cross section results for the electron impact electronic excitation from ground state to the $^3B_2$ and $^3A_1$ states of the furan molecule, we used three different models described in detail in the following. One of these models, hereafter referred as MODEL1, was constructed in order to include both transitions, *i.e.*, the $^1A_1 \rightarrow {}^3B_2$ and the $^1A_1 \rightarrow {}^3A_1$ excitations are considered in the same round of calculations and compete among themselves (and, of course, with excitations to the other states present in the space of coupled-channels, as listed in the first line of Table 1) for the flux that defines the cross sections. In this case, the active space for the

SCI calculation was composed by two holes (the b_1 and a_2 highest occupied orbitals) and two particles (a triplet IVO of the b_1 symmetry and a triplet IVO of the a_2 symmetry). Orbitals comprising the particle subspace were orthogonalized among themselves and with respect to all remaining IVOs through the usual Gram-Schmidt procedure. As a result we obtained two 4×4 matrices (eigenvectors and egeinvalues) for the overall $^2B_2$ and $^2A_1$ symmetries, being one for the triplet and another for the singlet Hamiltonians. By diagonaizing these matrices it was possible to provide a good description of the two low-lying triplet states ($^3B_2$ and $^3A_1$) of the target at the same time. Each of the other two models, in turn, include the excitation to only one of the excited states of interest: the $^1A_1 \rightarrow {}^3B_2$ transition is described according to MODEL2 and the $^1A_1 \rightarrow {}^3A_1$ transition according to MODEL3. It is worth noting that, again, all states included in the space of coupled-channels in MODEL2 (MODEL3) compete with the $^3B_2$ ($^3A_1$) state and with each other for the flux that define the cross sections. The steps in determining the active space of coupled-states was the same as above described, except for the fact that in MODEL2 the particle orbital subspace is composed by two orbitals of the b_1 type (a singlet and a triplet IVO out of the a_2 occupied orbital) and two IVOs of the a_2 type (a singlet and a triplet IVO out of the b_1 occupied orbital), whilst in MODEL3 it was composed by two orbitals of the b_1 type (a singlet and a triplet IVO out of the b_1 occupied orbital) and two IVOs of the a_2 type (a singlet and a IVO out of the a_2 occupied orbital). As can be seen from Table II, the energy values for the $^3B_2$ and $^3A_1$ excited states obtained by means of the MOB-SCI strategy (MODELs 1-3) shows to be in very good agreement with the experimental data and also with theoretical results coming from more sophisticated electronic structure calculations. On the other hand, the excitation energies related to transitions from ground state to the two singlet counterpart excited states, $^1B_2$ and $^1A_1$, were consistently higher (by more than 1 eV until around 2.2 eV) if compared to other data available in the literature. Here, it is important to recall that the small SCI calculation was carried so as to provide an accurate description of the first few low-lying excited states of furan. Higher excited states obtained within the scope of the MOB-SCI strategy should therefore be regarded as pseudo-states (i.e. states without an actual physical meaning) and for this reason they were not associated to any specific spectroscopy assignment.

In order to account for the polarization of the target we have adopted the following procedure: by freezing the occupied orbitals and the active particle orbitals described above, we

have diagonalized a +2 cationic Fock operator where two electrons are subtracted from the a_2 occupied orbital and generated modified virtual orbitals (MVOs) [54] from the remaining virtual orbitals. We then considered single excitations from all valence occupied orbitals to the MVOs with energies less than 10 Hartrees as a cut-off criterion for selection of the particle orbital space. The same set of MVOs were then used as scattering orbitals. We included singlet and triplet excitations which resulted in a total of of 19230 doublet CSFs divided per symmetry as follows: 5052 for A_1, 4581 for B_1, 5037 for B_2, and 4560 for A_2 for MODEL1; a total of of 18531 doublet CSFs divided per symmetry as follows: 4878 for A_1, 4391 for B_1, 4879 for B_2, and 4383 for A_2 for MODEL2 and a total of of 19230 doublet CSFs divided per symmetry as follows: 5064 for A_1, 4593 for B_1, 5025 for B_2, and 4548 for A_2 for MODEL3. Here it is important to mention that, although in all models we have used the same strategy for the treatment of polarization effects, the configuration state space obtained with the usual procedure is slightly different from one model to another. This difference occurs because the space of active states used to generate the CI-singles representation of the excited states of the target is different in each model. However it is important to note that, in all cases polarization effects were included in such a way to locate the resonances that appear in the elastic channel at the positions assigned as matching those observed in the literature (see, for instance, Refs. [21, 23, 24]). This aspect is of importance for theoretical models which involve electronic transitions to excited states for which the threshold is located at energies close to the position of resonances appearing in the elastic channel, as is the case of the $^3B_2$ and $^3A_1$ states of the furan molecule. A more detailed discussion on this subject can be found in Refs. [12, 13].

Using this procedure we obtained three models that, with respect to the orbital basis set and the description of polarization effects, are essentially equivalent. So, in principle, any discrepancy observed between the results obtained from different models reflects the fact that the multichannel coupling effects were included in a different way. That is, despite the scattering calculations for our three models were performed with the same number of coupled-channels (nine-state close-coupling level of approximation), the "type" of excited states and, as a consequence the position of the excitation thresholds are found to be different in each case. Also important to the discussion carried out below is the fact that the potential describing the electron-molecule interaction changes to the extent that each one of the excited states belonging to the coupled-channel space is included in the scattering calculations. In

fact, as can be seen below, the cross sections are so sensitive to the proximity of an excitation threshold such that we observe a sharp variations in the magnitude (for ICSs) and in shape (for DCSs) of the curves in the region around the energy corresponding to the opening of a given coupled-channel.

IV RESULTS AND DISCUSSION

Taking all these considerations in mind, in the next section we compare the data obtained from the three models described above with measurements taken earlier by our group [23].

(a) Elastic Scattering: The first results discussed are the DCSs for the elastic scattering at several representative E_0 values, shown in Figures 3 and 4. We note here that although the scattering calculations have been carried out to generate electronically inelastic cross sections for the $^1A_1 \rightarrow {}^3B_2$ and the $^1A_1 \rightarrow {}^3A_1$ transitions, the elastic contribution to the scattering amplitudes is also simultaneously computed since the elastic channel is included in the space of coupled-states. The results presented in Figure 3 show that the DCSs obtained using MODEL1, MODEL2 and MODEL3 are, baring some minor differences, very consistent with each other and also in very good agreement with the experimental data from Ref. [23]. The same level of agreement between all the three models considered in our study is observed for other energies in the range 0-30 eV (not shown here). These results show that the multichannel calculations carried out according to all the models used here provide elastic cross sections in very good agreement with the experiment. In Figure 4 we present a comparison for the elastic cross sections obtained in MODEL1 calculations performed at the static-exchange plus polarization (SEP) level of approximation with and without inclusion of channel-coupling. The importance in including multichannel effects for description of the elastic scattering at high energies is clearly highlighted by the improved agreement with experiment at 20 and 30 eV. At those energies the elastic DCSs are lowered due to the flux leakage to the now opened inelastic channels. This effect has also been obtained by using complex (absorption) potentials [55]. In order to give an indication of the net influence of channel-coupling effects on the elastic results, Figure 5 shows a symmetry decomposition of the elastic ICS, with and without

channel coupling. For all molecular symmetries shown, the ICS calculated under the single-channel model shows pseudo-resonances about the threshold energies of the excited states. In the multichannel calculation these are states kept open and the opening state can compete with the elastic for cross section flux. In the single-channel calculation where they are kept closed, the absence of this competition results in spurious spikes in the ICS.

(b) Electronic Excitation: The measured DCSs are tabulated for excitation of all states experimentally investigated and included in the unfolding analysis are shown in Table III ($^3B_2$) and Table IV ($^3A_1$), along with the corresponding ICSs. Theory for the triplet states is limited in energy range to $E_0 \leq 10\ eV$ due to the growing number of open channels with increasing E_0 values. Both measured and calculated DCSs of this work are shown for comparison in Figure 6 for all E_0 values for the excitation of the $^3B_2$ state from the ground state and in Figure 7 the excitation of the $^3A_1$ state. The quantitative agreement between the experiment and theory is reasonable, considering the complexity of the problem, at the lower E_0 values of 5 eV, 6 eV and 7.5 eV. However, none of the calculations reproduces the rapid drop in forward scattering observed in the experimental DCSs at these energies in the region of small for both states. At the energy of 10 eV the discrepancy among theoretical and experimental results is about a factor of three even though, in the case of the $^3B_2$ state, the shape of the DCS curve is similar. The MODEL1 DCSs show significantly better agreement with the experimental data for 10 eV than the others. The backward profile of the DCSs suggests that the excitation of these features is typical of that found in spin-exchange type scattering i.e. a singlet $\longleftrightarrow$ triplet excitation which is similar for both excitations.

ICS results for the study of the electronic excitation of furan by electron impact obtained from all the models MODEL1-3 are shown in Figures 8 and 9 for the excitation of the $^3B_2$ state and the $^3A_1$ state, respectively. Our calculated ICS curves display the presence of several structures, some of which are related to the opening of states that belongs to the space of coupled-channels included in the multi-state calculations employed. The threshold energies for these states are indicated by the arrows in Figures 8 and 9, where near to these thresholds we observe sharp variations in the magnitude of the ICSs. Other structures appearing at different energies may be related to core-excited shape resonances or may also be spurious, a careful investigation into these features is needed before any assignments are

made. Encouragingly, both theoretical results and experimental results show both compatible magnitudes and similar trends in the dependency of the integral cross section with the energy, at least at incident energies less than 10 eV. At the higher energy of 10 eV agreement is not as good with a difference of a factor of about 3.

V. CONCLUSIONS

In this work, we presented experimental and theoretical results for the excitation of the two lowest triplet states of furan by electron impact. Furan was chosen because it represents a simpler, but similar system to the 2-deoxyribose molecule, the sugar-like component of the DNA backbone and because it presents two prominent shape resonances around the excitation threshold of the $^3B_2$ state. After performing a series of tests to evaluate the numerical stability of our scattering calculations and also increase the grid resolution of energy points, we concluded that MODEL1 provides ICS and DCS cross sections which show better agreement overall with the experiment as compared to the other two models. Finally, we would like to call attention for the fact that the DNA nitrogenated bases, as well as many other organic molecules of biological or technological relevance, have excited states in the energy range from 3 to 5 eV. As a consequence, an adequate description of electron-impact electronic excitation to such low-lying states must necessarily be carried out with the inclusion of polarization effects of the target in order to provide reliable cross section values. In terms of experimental effort, it is important to continue such investigations at near threshold energies where it becomes possible for meaningful close-coupling multi-state models to work and to provide further tests for experiment, before both experiments and models can be extended to higher energies.

ACKNOWLEDGEMENTS

This work was funded through a collaborative program by the U.S. National Science Foundation under Grants No. PHY 0653452 and No. PHY 0653396 and by the Brazilian agency Conselho Nacional de Desenvolvimento Científico e Tecnológico (CNPq) under Project No. 490415/2007-5. R.F. da C., M.H.F.B., M.C.A. Lopes and M.A.P.L. acknowledge additional support from CNPq and from the Brazilian agencies Coordenação de Aperfeiçoamento de

Pessoal de Nível Superior (CAPES), Fundação de Amparo à Pesquisa do Estado de São Paulo (FAPESP), the Paraná state agency Fundação Araucária, Fundação de Amparo à Pesquisa do Estado de Minas Gerais (FAPEMIG) and Financiadora de Estudos e Projetos (FINEP) under Project No. CT-Infra 1. M.H.F.B. further acknowledges computational support from Professor Carlos M. de Carvalho at DF-UFPR. Computational support from Centro de Computação John David Rogers (CCJDR) and from Centro Nacional de Processamento de Alto Desempenho em São Paulo (CENAPAD), where the calculations in Brazil were performed, is gratefully acknowledged.

---

* Electronic address: romarly.costa@ufabc.edu.br

[1] B. Boudaïffa, P. Cloutier, D. Hunting, M. A. Huels, and L. Sanche, *Science* **287**, 1658 (2000).

[2] X. Pan, P. Cloutier, D. Hunting and L. Sanche, *Phys. Rev. Lett.* **90**, 208102 (2003).

[3] M. A. Huels, B. Boudaïffa, P. Cloutier, D. Hunting and L. Sanche, *J. Am. Chem. Soc.* **125**, 4467 (2003).

[4] F. Martin, P. D. Burrow, Z. Cai, P. Cloutier, D. Hunting and L. Sanche, *Phys. Rev. Lett.* **93**, 068101 (2004).

[5] L. Sanche, *Eur. Phys. J.* D **35**, 367 (2005).

[6] P. L. Levesque, M. Michaud, W. Cho, and L. Sanche, *J. Chem. Phys.* **122**, 224704 (2005).

[7] F. A. Gianturco, F. Sebastianelli, R. R. Lucchese, I. Baccarelli, and N. Sanna, *J. Chem. Phys.* **128**, 174302 (2008).

[8] C. Winstead and V. McKoy, *J. Chem. Phys.* **125**, 174304 (2006).

[9] A. Dora, J. Tennyson, L. Bryjko, and T. van Mourik, *J. Chem. Phys.* **130**, 164307 (2009).

[10] M. Bazin, M. Michaud, and L. Sanche, *J. Chem. Phys.* **133**, 155104 (2010).

[11] M. Michaud, M. Bazin, and L. Sanche, *Int. J. Rad. Bio.* **88**, 15 (2012).

[12] R. F. da Costa, M. H. F. Bettega and M. A. P. Lima, *Phys. Rev.* A **77**, 012717 (2008).

[13] R. F. da Costa, M. H. F. Bettega and M. A. P. Lima, *Phys. Rev.* A **77**, 042723 (2008).

[14] M. Allan, C. Winstead and V. McKoy, *Phys. Rev.* A **77**, 042715 (2008).

[15] See, for instance, T. Fleig, S. Knecht, and C. Hättig, *J. Phys. Chem.* A **111**, 5482 (2007) and references therein.

[16] C. S. Trevisan, A. E. Orel, and T. N. Rescigno *Phys. Rev.* A **70**, 012704 (2004); C. Winstead

and V. McKoy, *Phys. Rev. Lett.* **98**, 113201 (2007); E. M. de Oliveira, M. A. P. Lima, M. H. F. Bettega, S. d'A. Sanchez, R. F. da Costa, and M. T. do N. Varella, *J. Chem. Phys.* **132**, 204301 (2010); Z. Masin and J. D. Gorfinkiel, *J. Chem. Phys.* **135**, 144308 (2011) and references therein.

[17] E. H. van Veen, *Chem. Phys. Lett.* **41**, 535 (1976).

[18] W. M. Flicker, O. A. Mosher and A. Kuppermann, *Chem. Phys. Lett.* **38**, 489 (1976).

[19] W. M. Flicker, O. A. Mosher and A. Kuppermann, *J. Chem. Phys.* **64**, 1315 (1976).

[20] M. V. Muftakhov, N. L. Asfandiarov, and V. I. Khvostenko, *J. Electron Spectrosc. Relat. Phenom.* **69**, 165 (1994); V. I. Khvostenko, A. S. Vorobyov, and O. G. Khvostenko, *J. Phys.* B **23**, 1975 (1990).

[21] A. Modelli and P. W. Burrow, *J. Phys. Chem.* A **108**, 5721 (2004).

[22] M. H. F. Bettega and M. A. P. Lima, *J. Chem. Phys.* **126**, 194317 (2007).

[23] M. Khakoo, J. Muse, K. Ralphs, R. F. da Costa, M. H. F. Bettega and M. A. P. Lima, *Phys. Rev.* A **81**, 062716 (2010)

[24] C. Szmytkowski, P. Moejko, E. Ptasińka-Denga and A. Sabisz, *Phys. Rev.* A **82**, 032701 (2010).

[25] P. Sulzer et al., *J. Chem. Phys.* **125**, 044304 (2006).

[26] F. Motte-Tollet, G. Eustatiu, and D. Roy, *J. Chem. Phys.* **105**, 7448 (1996).

[27] M. Dampc and M. Zubek, *Int. J. Mass Spectrom.* **277**, 52 (2008).

[28] L. Hargreaves, L. Albaridy, G. Serna, M. C. A. Lopes, M. A. Khakoo, *Phys. Rev.* A **84**, 062705, (2011).

[29] K. Takatsuka and V. McKoy, Phys. Rev. A **24**, 2473 (1981); *Phys. Rev.* A **30**, 1734 (1984).

[30] M. H. F. Bettega, L. G. Ferreira, and M. A. P. Lima, *Phys. Rev.* A **47**, 1111 (1993).

[31] M. A. Khakoo, C. E. Beckmann, S. Trajmar, and G. Csanak, *J. Phys.* B **27**, 3159 (1994).

[32] J. H. Brunt, G. C. King, and F. H. Read, *J. Phys.* B **10**, 1289 (1977).

[33] M. A. Khakoo, H. Silva, J. Muse, M. C. A. Lopes, C. Winstead, and V. McKoy, *Phys. Rev.* A **78**, 052710 (2008).

[34] M. Hughes, K. E. James Jr., J. G. Childers, and M. A. Khakoo, *Meas. Sci. Technol.* **14**, 841 (1994).

[35] L. R. Le Clair, S. Trajmar, *J. Phys.* B. **29**, 5543 (1996).

[36] D. V. Fursa and I. Bray, *Phys. Rev.* A **52**, 1279 (1995).

[37] E. Schow, K. Hazlett, J. G. Childers, C. Medina, G. Vitug, I. Bray, D. V. Fursa and M. A.

Khakoo, *Phys. Rev.* A **72**, 062717 (2005).

[38] A. Guiliani and M. J. Hubin-Franskin, *Int. J. Mass Spec.* **205**, 163 (2001).

[39] http://www.soft.proindependent.com/qtiplot.html.

[40] R. F. da Costa, F. J. da Paixão, and M. A. P. Lima, *J. Phys.* B **37** L129 (2004); *J. Phys.* B **38** 4363 (2005).

[41] G. B. Bachelet, D. R. Hamann, and M. Schlüter, *Phys. Rev.* B **26**, 4199 (1982).

[42] P. Chaudhuri, M. T. do N. Varella, C. R. C. Carvalho, and M. A. P. Lima, *Nucl. Instrum. Methods Phys. Res.* B **221** 69 (2004); *Phys. Rev.* A **69** 042703 (2004).

[43] *CRC Handbook of Chemistry and Physics*, 79th ed., edited by D. R. Lide (CRC, Boca Raton, 1998).

[44] M. H. F. Bettega, A. P. P. Natalense, M. A. P. Lima, and L. G. Ferreira, *Int. J. Quantum Chem.* **60**, 821 (1996).

[45] T. H. Dunning Jr., *J. Chem. Phys.* **53**, 2823 (1970).

[46] W. J. Hunt and W. A. Goddard, *Chem. Phys. Lett.* **3**, 414 (1969).

[47] H. Nakatsuji, O. Kitao, and T. Yonezawa, *J. Chem. Phys.* **83**, 723 (1985).

[48] L. Serrano-Andres, M. Merchan, I. Nebot-Gil, B. O. Roos, and M. Fulscher, *J. Am. Chem. Soc.* **115**, 6184 (1993).

[49] M. H. Palmer, I. C. Walker, C. C. Ballard, and M. F. Guest, *Chem. Phys.* **192**, 111 (1995).

[50] M. H. Palmer, I. C. Walker, and M. F. Guest, *Chem. Phys.* **238**, 179 (1998).

[51] H. Nakano, T. Tsuneda, T. Hashimoto, and K. Hirao, *J. Chem. Phys.* **104**, 2312 (1996).

[52] J. Wan, J. Meller, M. Hada, M. Ehara, and H. Nakatsujia, *J. Chem. Phys.* **113**, 7853 (2001).

[53] A. Kokalj, *J. Mol. Graph. Model.* **17**, 176 (1999).

[54] C. W. Bauschlicher, *J. Chem. Phys.* **72**, 880 (1980).

[55] E. A. y Castro, G. L. C. de Souza, I. Iga, L. E. Machado, L. M. Brescansin, and M.-T. Lee, *J. Electron Spectrosc. Rel. Phenom.* **159**, 30 (2007).

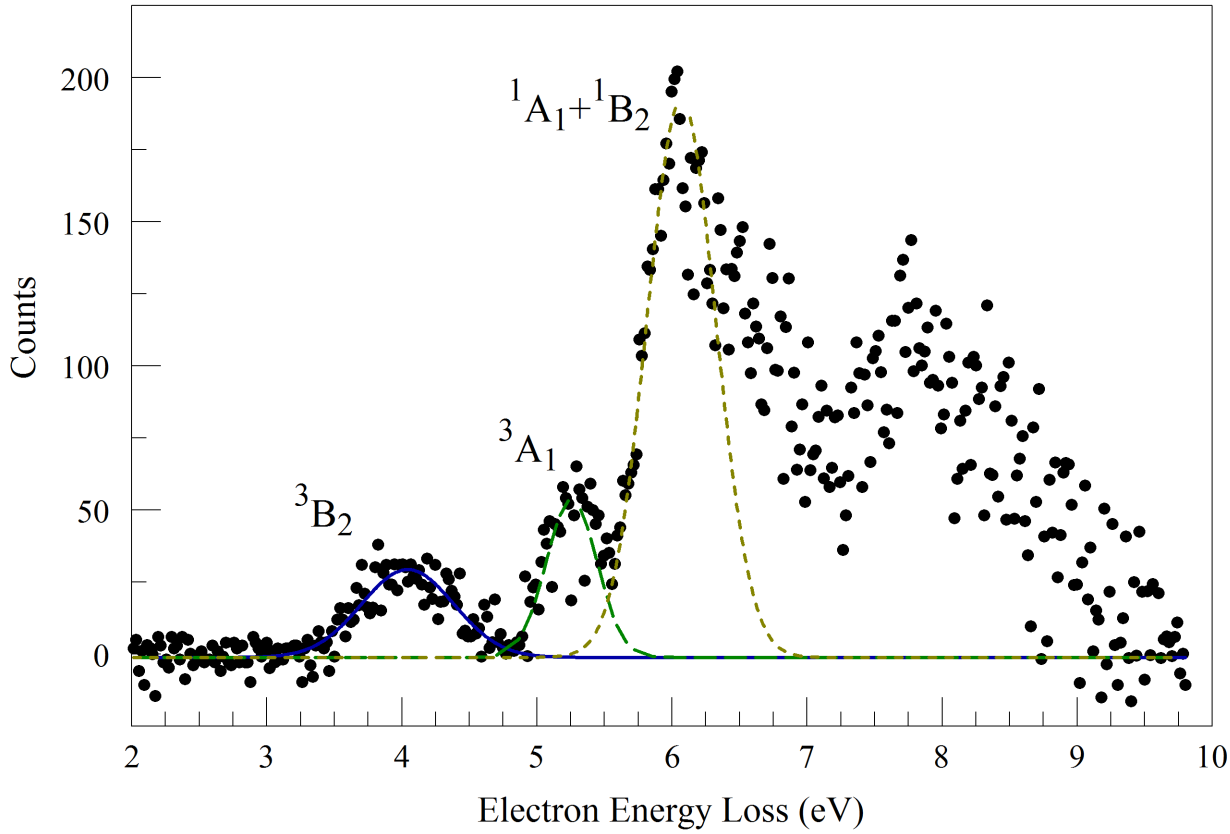

FIG. 1: (Color online) Background subtracted electron energy loss spectrum of furan at the higher E_0 of 10.0 eV and $\theta = 40°$. The dotted lines are Gaussian fits used to unfold the individual electronic states (labeled).

		Energy (eV)							
	1-channel	2-channel	3-channel	4-channel	5-channel	6-channel	7-channel	8-channel	9-channel
MODEL1	Elastic	3.68	5.12	7.72	7.74	8.39	8.55	10.97	11.03
MODEL2	Elastic	3.66	7.20	8.47	8.87	9.76	10.93	14.89	15.53
MODEL3	Elastic	5.10	7.64	8.36	11.01	14.90	16.14	17.63	18.08

TABLE I: Energy thresholds (in eV) of the states composing the space of coupled-channels.

State	Energy (eV)						
	This work			Theory			Experiment[a]
	MODEL1	MODEL2	MODEL3	CASPT2[b]	MRDCI[c]	SAC-CI[d]	
$^3B_2$	3.68	3.66	—	3.99	3.93	4.39	3.99
$^3A_1$	5.12	—	5.10	5.15	5.28	5.63	5.15
$^1B_2$	7.72	7.20	—	6.04	6.88	6.40	6.04
$^1A_1$	8.39	—	8.36	6.16	6.63	6.79	—

[a]Experimental data were taken from Refs [47–51] and references therein.
[b]Reference [47]
[c]Reference [48]
[d]Reference [52]

TABLE II: Comparison of the excitation energies (in eV) for furan, as obtained by several theoretical methods with experiment.

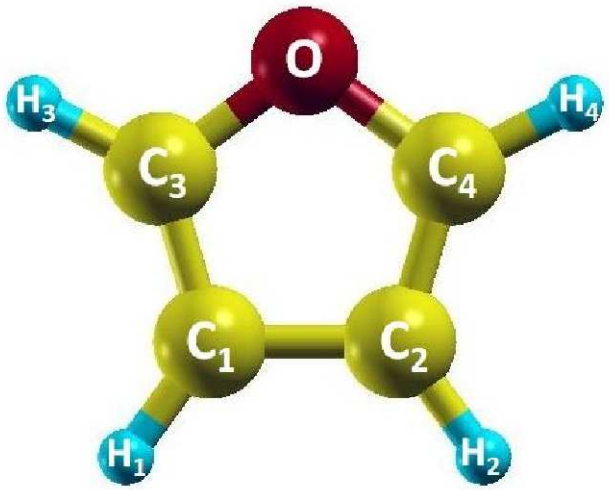

FIG. 2: (Color online) Ball and stick model structure of furan (C_4H_4O) obtained with the XCrysDen^{TM} (Crystalline Structures and Densities) software [53].

Scattering Angle	5 eV	6 eV	7.5 eV	10 eV	15 eV
10°			0.49 (0.21)	0.79 (0.15)	0.36 (0.07)
15°			1.66 (0.30)		0.40 (0.09)
20°		0.89 (0.19)	2.40 (0.40)	1.49 (0.28)	0.47 (0.09)
25°		1.29 (0.23)	1.65 (0.34)		0.44 (0.08)
30°		1.88 (0.36)	2.22 (0.37)	1.39 (0.28)	0.53 (0.10)
35°	0.38 (0.22)	2.53 (0.40)			0.67 (0.11)
40°	0.74 (0.24)	2.66 (0.46)	3.18 (0.52)	1.73 (0.27)	0.69 (0.12)
50°	1.15 (0.22)	3.00 (0.49)	3.56 (0.59)	1.72 (0.29)	0.79 (0.15)
60°	1.47 (0.22)	3.46 (0.53)	3.53 (0.58)	1.99 (0.32)	0.79 (0.14)
70°				2.03 (0.32)	0.67 (0.11)
80°	1.81 (0.30)	5.18 (0.87)	5.59 (0.95)		0.68 (0.12)
90°	1.83 (0.26)	5.03 (0.80)	6.39 (1.07)	2.32 (0.31)	0.63 (0.12)
105°	1.93 (0.32)	4.49 (0.72)	6.75 (1.13)	2.37 (0.39)	0.77 (0.14)
120°	1.96 (0.34)	4.52 (0.71)	5.81 (0.95)	2.94 (0.49)	0.87 (0.15)
130°	2.02 (0.32)	4.91 (0.87)	5.88 (0.99)	3.54 (0.51)	1.10 (0.18)
ICS	20.2 (6.90)	52.4 (15.7)	63.8 (15.0)	31.4 (6.70)	11.0 (2.1)

TABLE III: Measured DCS and ICS data for excitation from the ground state to the $^3B_2$ state of furan by electron impact, in units of 10^{-18}cm^{2}sr^{-1} (DCS) and 10^{-18}cm^2 (ICS). The absolute uncertainties are shown in parentheses.

Scattering Angle	7.5 eV	10 eV	15 eV
10°		0.83 (0.12)	0.88 (0.14)
15°	3.30 (0.52)		0.76 (0.12)
20°	5.60 (0.77)	1.53 (0.22)	0.86 (0.17)
25°	1.93 (0.46)		0.76 (0.12)
30°	2.62 (0.44)	1.13 (0.20)	0.73 (0.12)
35°			0.97 (0.16)
40°	3.41 (0.56)	1.49 (0.20)	0.92 (0.16)
50°	3.59 (0.60)	1.68 (0.23)	0.91 (0.18)
60°	4.40 (0.70)	2.01 (0.30)	0.93 (0.16)
70°			0.73 (0.13)
80°	7.11 (1.18)	2.19 (0.33)	0.69 (0.12)
90°	8.72 (1.38)	1.96 (0.25)	0.71 (0.12)
105°	8.84 (1.41)	2.24 (0.34)	0.70 (0.15)
120°	7.39 (1.15)	2.38 (0.36)	0.93 (0.16)
130°	7.00 (1.16)	2.75 (0.37)	1.32 (0.21)
ICS	78.7 (13.0)	27.3 (4.10)	12.8 (2.70)

TABLE IV: Measured DCS and ICS data for excitation from the ground state to the $^3A_1$ state of furan by electron impact, in units of 10^{-18}cm^{2}sr^{-1} (DCS) and 10^{-18}cm^2 (ICS). The absolute uncertainties are shown in parentheses.

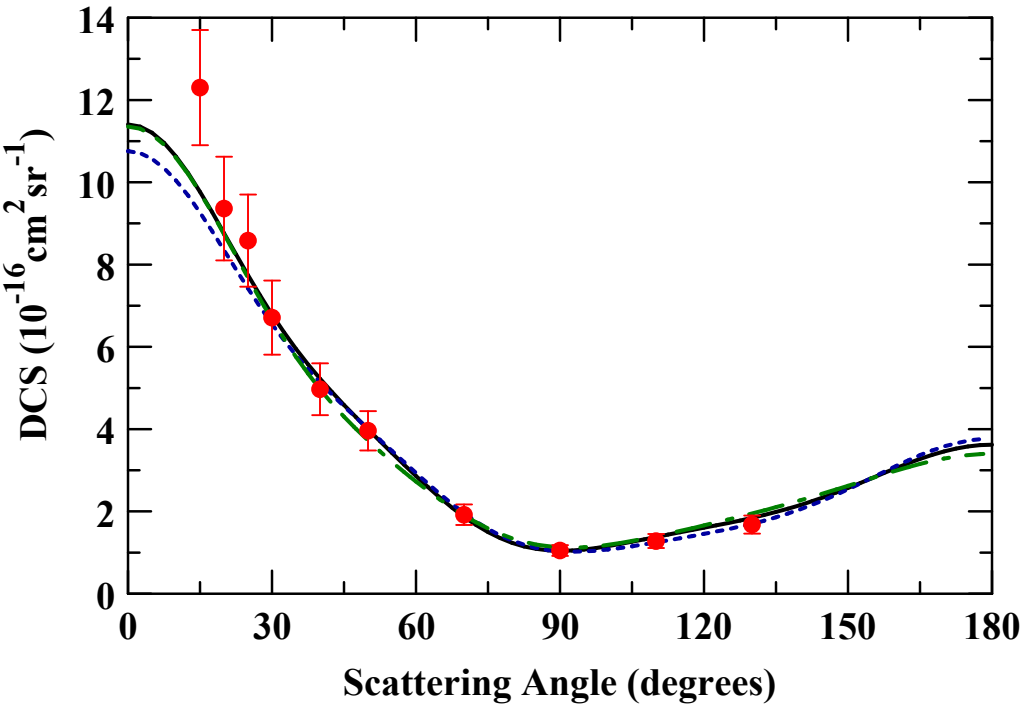

FIG. 3: (Color online) Differential cross sections for elastic electron scattering from furan at the E_0 value of 5.0 eV. Shown are the measurements of Khakoo *et al.* [23], and theoretical predictions from the three models considered in this study, labeled MODEL 1 (black solid curve), MODEL 2 (blue dashed curve) and MODEL 3 (green dash-dot curve).

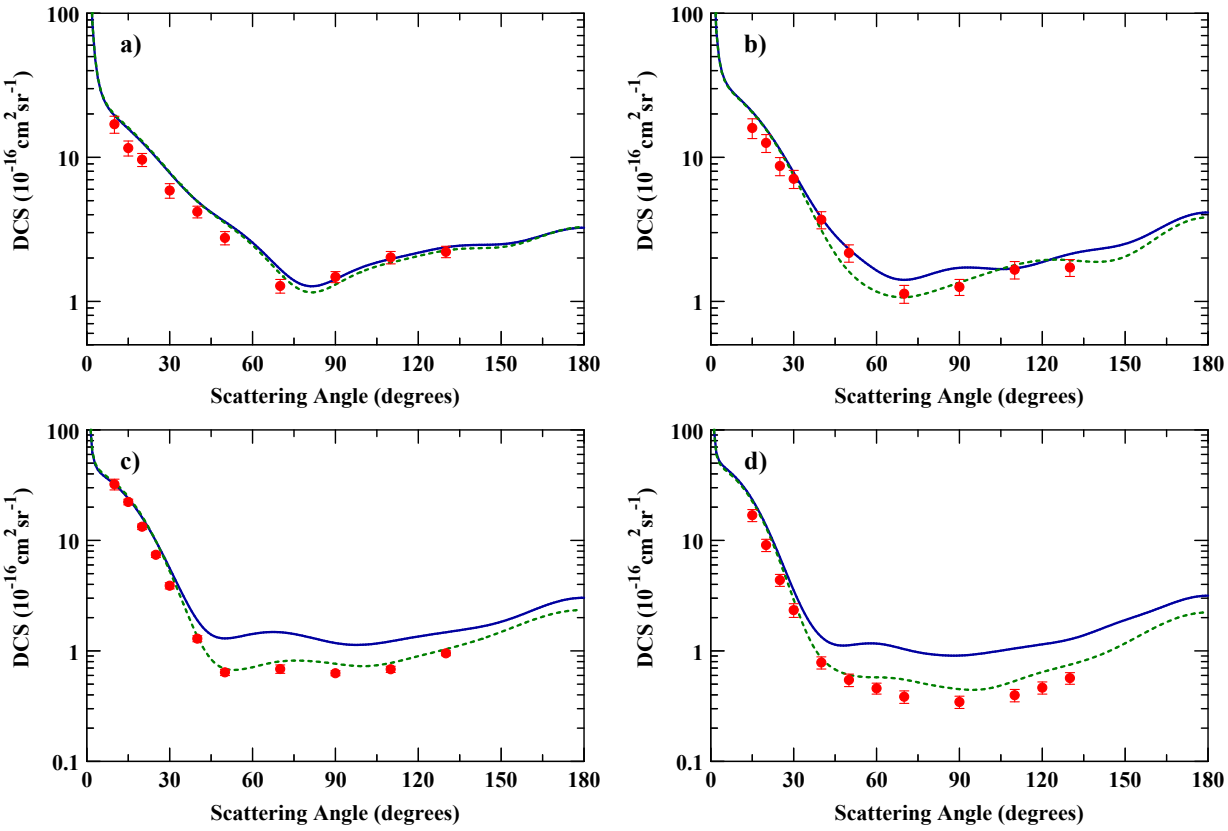

FIG. 4: (Color online) Differential cross section for elastic electron scattering from furan at E_0 values of 7 eV (a), 10 eV (b), 20 eV (c) and 30 eV (d). Shown are the measurements of Khakoo et al. [23] (closed red circles) and theoretical results from the present Schwinger multichannel calculations at the static-exchange plus polarization level (blue solid curve) and with the addition of multichannel coupling effects (green dashed curve).

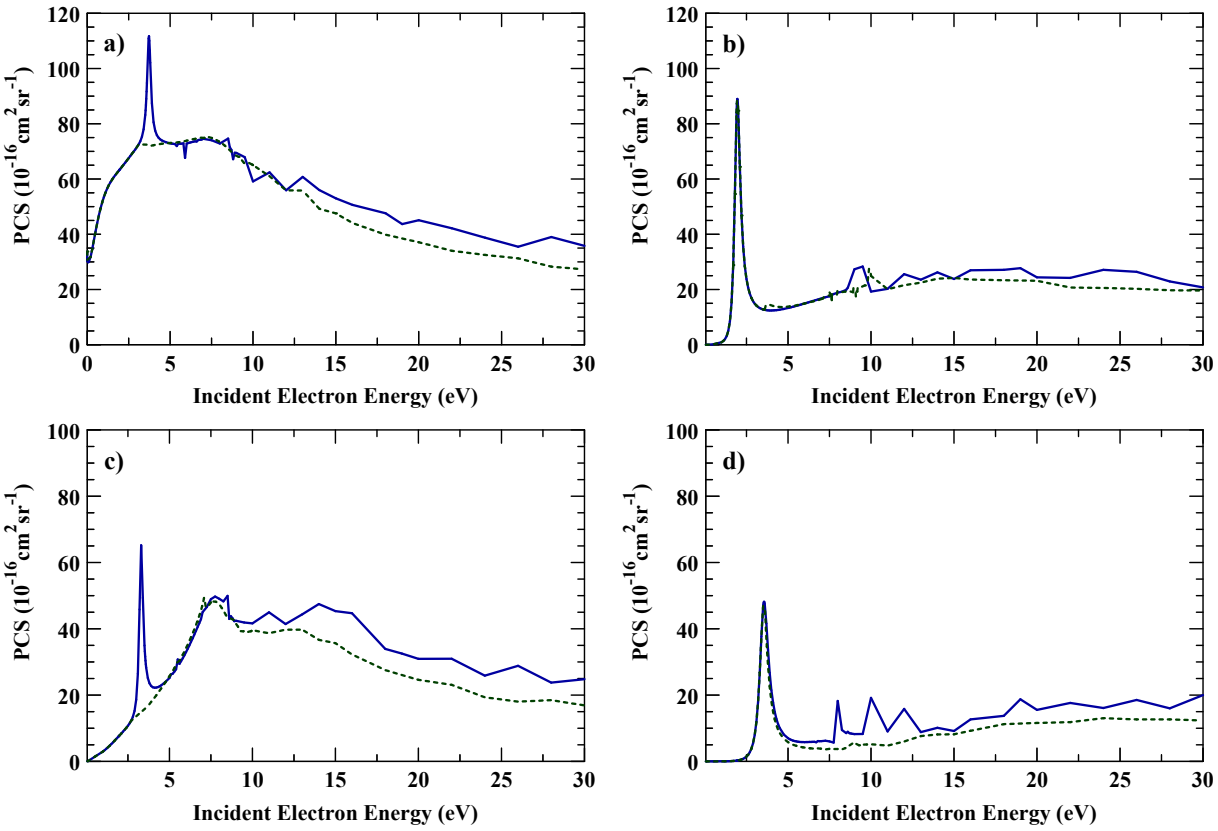

FIG. 5: (Color online) Comparisons between integral cross sections for elastic electron scattering from furan determined by models without (blue solid curve) and with (green dashed curve) multichannel coupling. The molecular symmetries shown are (a) A_1, (b) B_1, (c) B_2 and (d) A_2. See text for discussion.

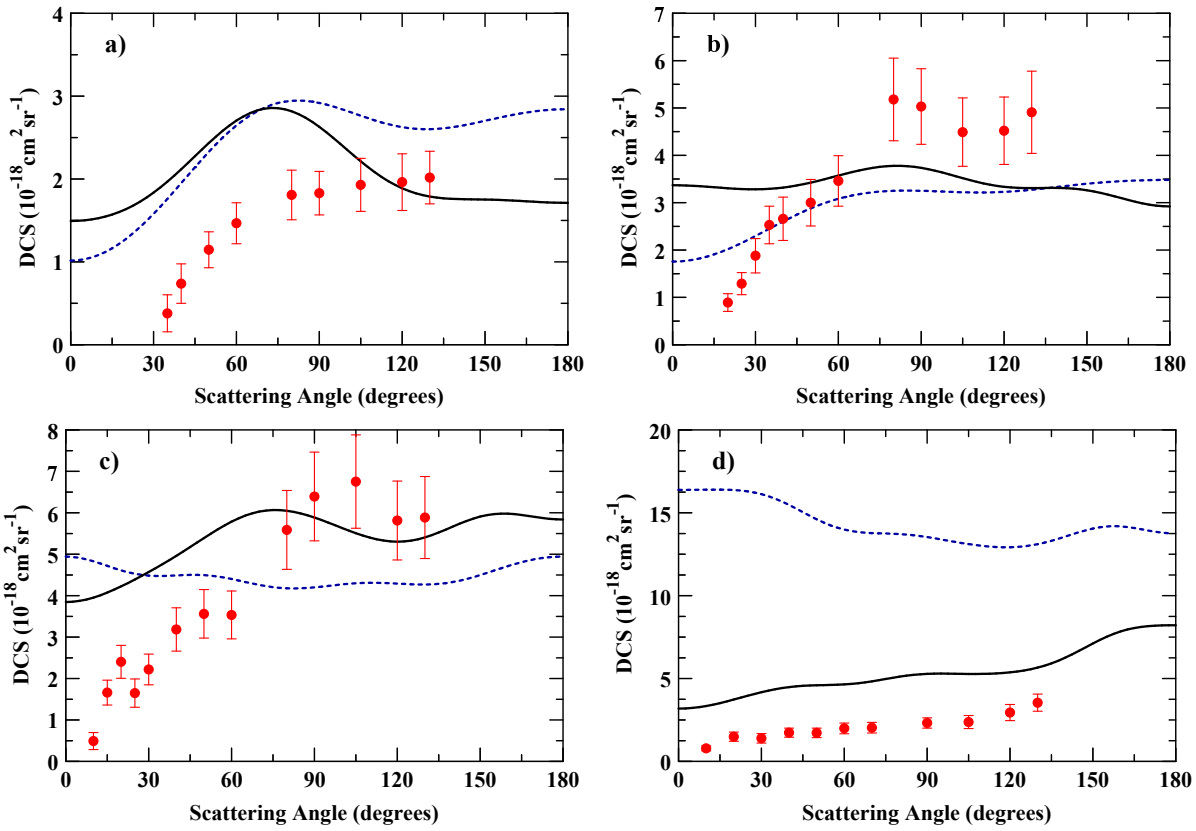

FIG. 6: (Color online) Differential cross section for the electronic excitation from ground state to the $^3B_2$ state of furan by electron impact at the energy of 5 eV (a), 6 eV (b), 7.5 eV (c) and 10 eV (d). The present experimental data (full circles) are shown, as well as the present theoretical results from MODEL 1 (black solid curve) and MODEL 2 (blue dashed curve).

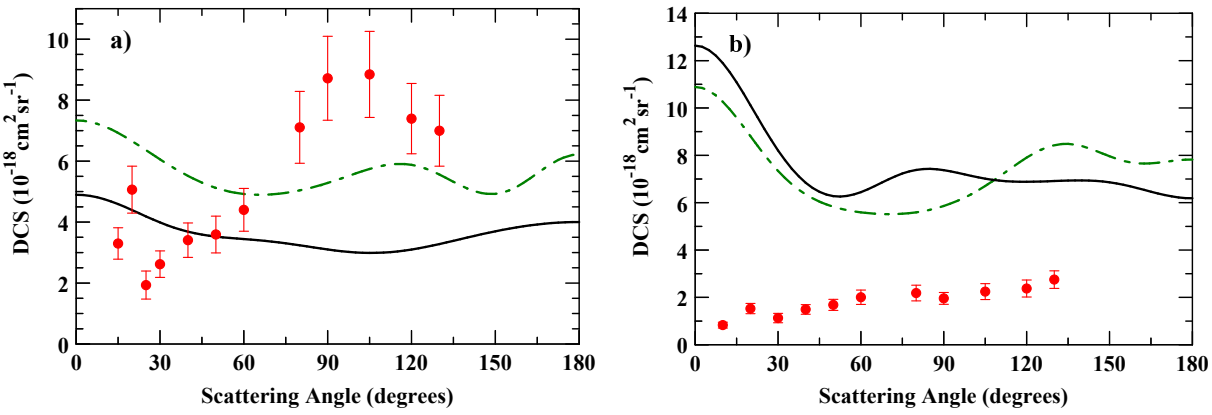

FIG. 7: (Color online) Differential cross section for the electronic excitation from ground state to the $^3A_1$ state of furan by electron impact, at incident energies of 7.5 eV (a) and 10 eV (b). The present experimental data points (red circles) are shown, as well as the present theoretical results from MODEL 1 (black solid curve) and MODEL 3 (green dash-dot curve).

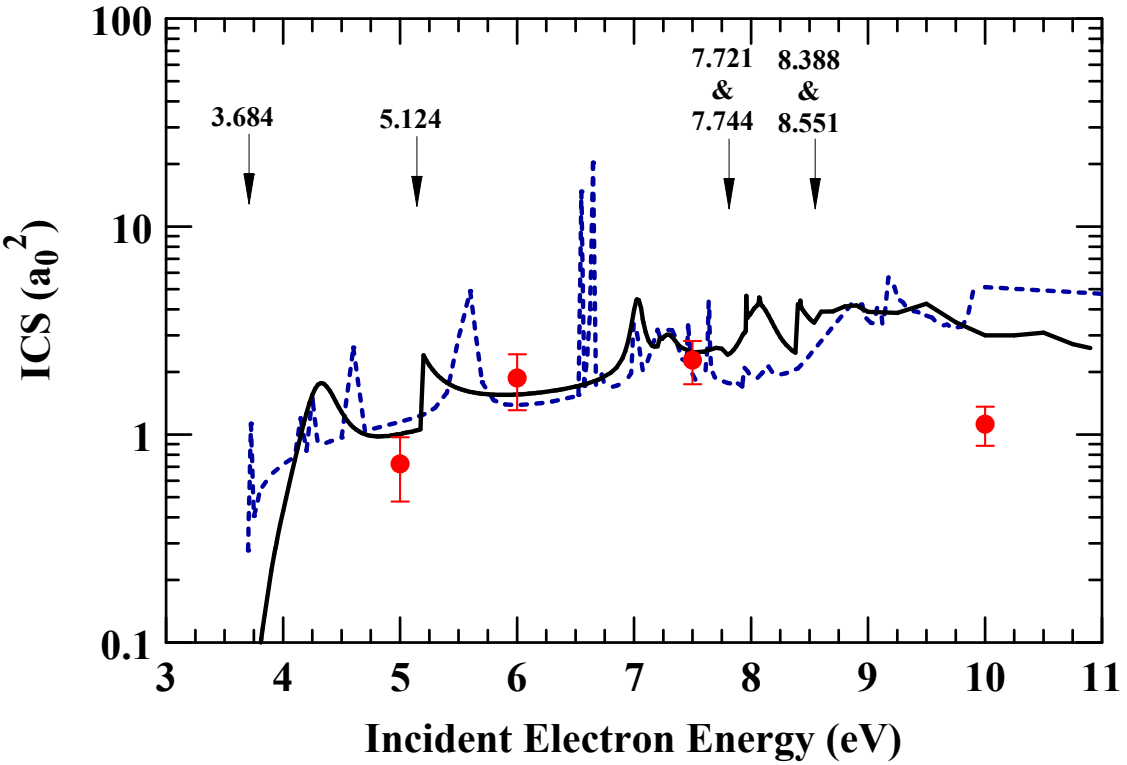

FIG. 8: (Color online) Integral cross section for the electronic excitation from ground state to the $^3B_2$ state of furan by electron impact. Shown are the present experimental data (full circles) and theoretical results from MODEL 1 (black solid curve) and MODEL 2 (blue dashed curve).The arrows indicate the energy thresholds of the states included in the space of coupled-channels as listed in the first line of Table 1.

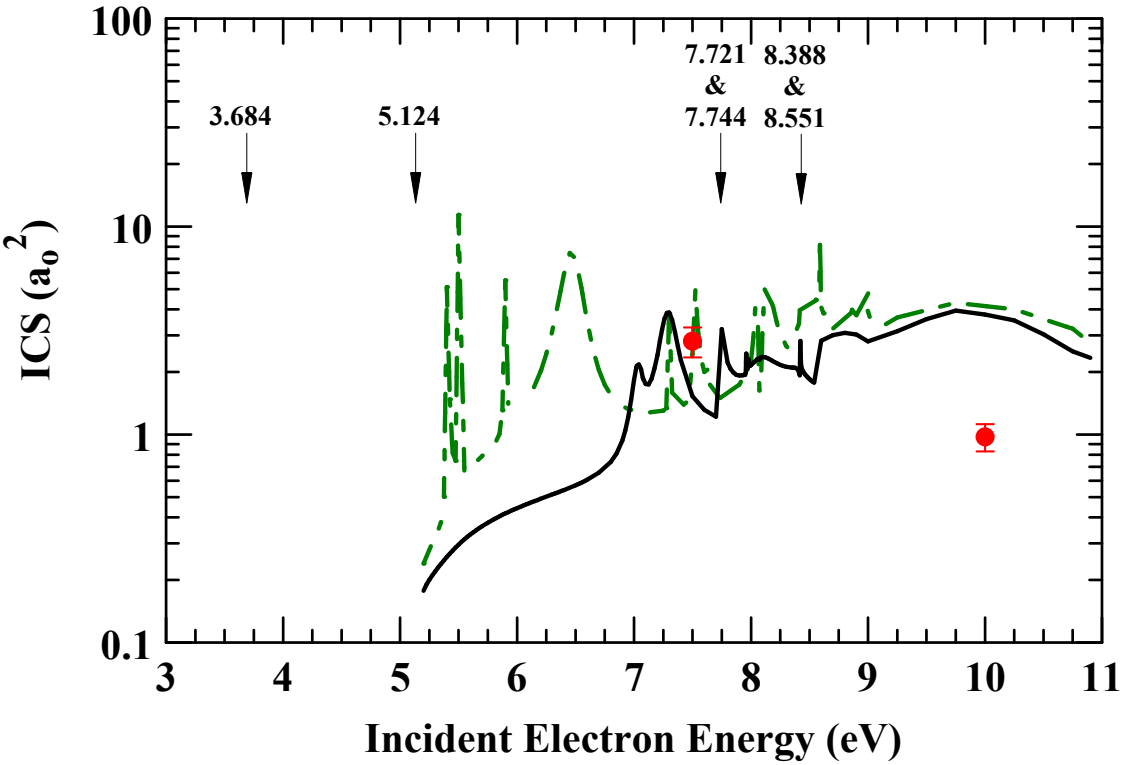

FIG. 9: (Color online) Integral cross section for the electronic excitation from ground state to the $^3A_1$ state of furan by electron impact. Shown are the present experimental data (full circles) and theoretical results from MODEL 1 (black solid curve) and MODEL 3 (green dash-dot curve). The arrows indicate the energy thresholds of the states included in the space of coupled-channels as listed in the first line of Table 1.